Received: 9 November 2023 | Revised: 2 December 2023 | Accepted: 5 December 2023

DOI: 10.1002/jmor.21667

RESEARCH ARTICLE

JOURNAL OF morphology WILEY

Serial block-face scanning electron microscopy of the tail tip of post-metamorphic amphioxus finds novel myomeres with odd shapes and unusually prominent sclerocoels

Nicholas D. Holland | Linda Z. Holland

Marine Biology Research Division, Scripps Institution of Oceanography, University of California at San Diego, La Jolla, California, USA

Correspondence
Nicholas D. Holland, Marine Biology Research Division, Scripps Institution of Oceanography, University of California at San Diego, La Jolla, CA 92092, USA.
Email: nholland@ucsd.edu

Funding information
National Science Foundation, Grant/Award Number: IOS 1952567

Abstract

Serial block-face scanning electron microscopy of the tail tip of post-metamorphic amphioxus (*Branchiostoma floridae*) revealed some terminal myomeres never been seen before with other techniques. The morphology of these myomeres differed markedly from the chevron shapes of their more anterior counterparts. Histologically, these odd-shaped myomeres ranged from empty vesicles bordered by undifferentiated cells to ventral sacs composed of well-developed myotome, dermatome, and sclerotome. Strikingly, several of these ventral sacs gave rise to a nipple-like dorsal projection composed either entirely of sclerotome or a mixture of sclerotome and myotome. Considered as a whole, from posterior to anterior, these odd-shaped posterior myomeres suggested that their more substantial ventral part may represent the ventral limb of a chevron, while the delicate projection represents a nascent dorsal limb. This scenario contrasts with formation of chevron-shaped myomeres along most of the antero-posterior axis. Although typical chevron formation in amphioxus is surprisingly poorly studied, it seems to be attained by a dorso-ventral extension of the myomere accompanied by the assumption of a V-shape; this is similar to what happens (at least superficially) in developing fishes. Another unusual feature of the odd-shaped posterior myomeres of amphioxus is their especially distended sclerocoels. One possible function for these might be to protect the posterior end of the central nervous system from trauma when the animals burrow into the substratum.

KEYWORDS
Branchiostoma floridae, Cephalochordata, lancelet, myomeres, somites

1 | INTRODUCTION

Of the three chordate subphyla, Cephalochordata (commonly called amphioxus) is the sister group of Tunicata plus Vertebrata (Delsuc et al., 2008) and is evolving exceptionally slowly (Yue et al., 2014). These features make amphioxus a useful proxy for the invertebrate chordate ancestor of the vertebrates and a source of insights into how relatively simple characters served as points of departure for evolution of vertebrate complexity. Amphioxus structures studied from this viewpoint include the dorsal nerve cord, notochord, pharyngeal slits, and the somites that develop into segmentally arranged myomeres and are the subject of the present contribution.

During embryonic and larval development of amphioxus, formation of the segmented musculature begins with production of somites, each of which is a small cluster of undifferentiated looking cells. The somites arise from anterior to posterior along either side of

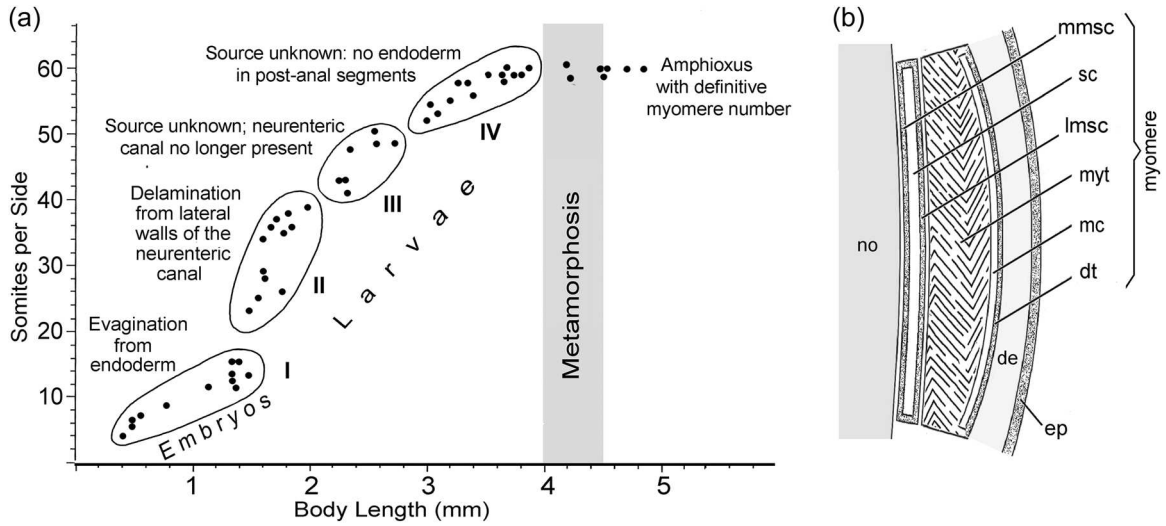

FIGURE 1 *Branchiostoma floridae*. (a) Increase in somite number along one side of the body during development (data from Stokes, 1996). Phases I–IV of somite formation are explained in Section 4.1. (b) Diagrammatic cross-sectional view of a myomere (not flexed into a chevron to facilitate drawing) in the context of nearby notochord (no), dermis (de), and epidermis (ep). From medial to lateral, the myomere comprises: mmsc, medial mesothelium of sclerocoel; sc, sclerocoel; lmsc, lateral mesothelium of sclerocoel; myt, myotome; mc, myocoel; and dt, dermatome.

the lengthening body (Figure 1a) by processes discussed in Section 4.1 During larval development, each somite generates several constituent tissues to become a myomere (Figure 1b) and contemporaneously morphs into a chevron shape. The number of myomeres reaches a species-specific maximum shortly before the onset of metamorphosis. For example, Howell (1964) showed that adults of the Tampa population of the Florida amphioxus have a mean of 59 somites per side (range 57–61; $n = 100$).

Specifically, the present study describes the three-dimensional (3D) fine structure of the most posterior myomeres in the body of the Florida amphioxus as reconstructed from serial block-face scanning electron microscopy (SBSEM). We were surprised to discover that these myomeres look more like surrealist art objects than the nested series of progressively smaller chevrons that we expected to find there. Because the present study concerns post-metamorphic specimens, no new myomeres were still being added. Despite this static situation, however, differences among the posteriormost myomeres permit a plausible discussion of their dynamic qualities (in Section 4.1) from a developmental point of view. The discussion also considers the conspicuously dilated regions of sclerotome in the most posterior myomeres and speculates on a possible function for this feature.

2 | MATERIALS AND METHODS

2.1 | SBSEM and 3D reconstruction of fine structure

Specimens of the Florida amphioxus, *Branchiostoma floridae* Hubbs (1922), were obtained from a breeding colony maintained at Scripps Institution of Oceanography (Holland & Li, 2021). Three post-metamorphic specimens (1.1 cm long) selected for the present study were photographed alive by light microscopy—first at low magnification showing the entire body in left-hand view and second at high magnification showing details near the tail tip. Two of the specimens were poorly oriented in the block and their sectioning was terminated early (but not before showing that their detailed structure was virtually identical with that of the best oriented specimen described here).

For SBSEM, the posterior 2 mm of the body was cut off and transferred to the primary fixative composed of 0.15 mol l^{-1} cacodylate buffer [pH 7.4] containing 2% formaldehyde, 1.5% glutaraldehyde, and 2 mmol l^{-1} $CaCl_2$ at 4°C for 10 days (Deerinck et al., 2010). Subsequent postfixation steps (reduced osmium tetroxide, thiocarbohydrazide, osmium tetroxide, uranyl acetate, and lead aspartate) were as detailed in Wanner et al. (2016). Following dehydration in ethanol, specimens were transferred through acetone and embedded in Durcupan resin. We oriented the embedded specimens to yield a series of block-face images, starting at the tail tip.

Each sample was mounted in a Zeiss Merlin SEM and imaged in a 3 View Gatan system. The key feature for this procedure is the inclusion of an ultramicrotome in the SEM specimen chamber (Kornfeld & Denk, 2018). The block-face is scanned and recorded as a backscattered image; then the microtome shaves away a thin layer (for our work, 0.25 µm) from the block, thus exposing a new surface for imaging. The alternative scanning and shaving generate a series of block-face images, each superficially resembling a conventional transmission electron micrograph (TEM), although at moderately low resolution.

The best-oriented specimen yielded 3200 consecutive images, spanning 800 µm. Over the posterior third of this interval, the image of the whole animal fit within the 120 × 120 µm field of view.

However, as the dimensions of the animal progressively enlarged anteriorly, we were limited to viewing only the dorsal nerve cord and surrounding tissues. Thus, it was necessary to estimate the overall shape of the incomplete myomeres from light microscopic images of the same region (Figure 1b).

The entire SBSEM data set was converted to 3D images with the Reconstruct program, obtainable gratis from the web site of the Neural Systems Laboratory, Sargent College, Boston University (Borrett & Hughes, 2016; Fiala, 2005). After exposing our most anterior block face (number 3200), we montaged all of it to obtain a complete transverse view of the animal halfway along the postanal region. The montage was approximately at the boundary between the more familiar anterior myomeres and the unusually shaped ones at the tail end of the body.

2.2 | Convention for naming the posterior myomeres

In the present study, we have named the posterior myomeres according to the following convention: on the left, the most posterior one is designated LT (left terminal) followed by LT−1 (i.e., left terminal minus one), LT−2, LT−3, LT−4, and LT−5. Similarly, on the right, the myomeres are designated RT, RT−1, RT−2, RT−3, and RT−4. This terminology will be used below in describing the montage (Section 3.2), the left posterior myomeres (Section 3.3), and the right posterior myomeres (Section 3.4). As mentioned above, we detected no difference in the morphology of the posteriormost myomeres among three post-metamorphic individuals of *B. floridae*. Moreover, because of the unusually high degree of similarity in the morphology and its molecular genetic basis throughout the genus *Branchiostoma* (Carvalho et al., 2021; Somorjai et al., 2008), it would not be surprising to find similarly constructed posteriormost myomeres in all the congeners in the group. Finally, all the block-face images illustrated here are looked at from the tail end of the animal—therefore, left-side structures are on the left, and right-side structures are on the right.

2.3 | Criterion for distinguishing ventral and dorsal regions of myomeres

The typical myomeres along most of the body axis are shaped like chevrons with anterior facing points. In a side view, these points (one is indicated by an asterisk in Figure 2b) closely coincide with the ventral edge of the dorsal nerve cord. Thus, the dorsal and ventral limbs of the chevron are, respectively, dorsal and ventral to this landmark. At the tail end of the body, the level of the ventral edge of the dorsal nerve cord is also a convenient marker for distinguishing ventral and dorsal regions of the odd-shaped myomeres.

3 | RESULTS

3.1 | Light-microscopic context for the tail region studied

Figure 2a shows a living, post-metamorphic amphioxus in left-side view; the boxed area at its posterior end is enlarged as Figure 2b.

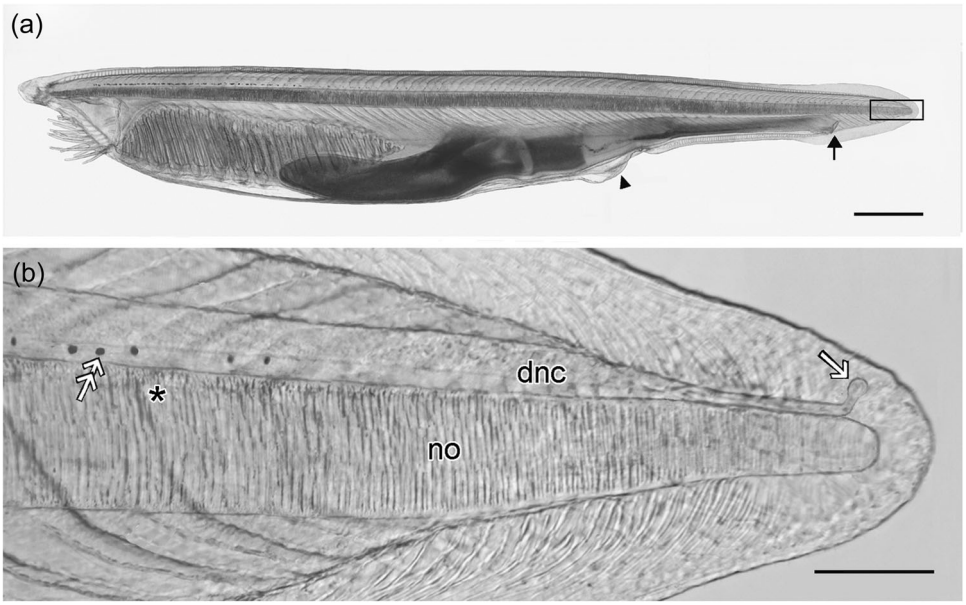

FIGURE 2 *Branchiostoma floridae*. (a) Light-microscopic image of a post-metamorphic living specimen in left-side view. The arrowhead and arrow indicate, respectively, atriopore and anus. The rectangle at the tail tip corresponds to the area of higher magnification in Figure 2b. Scale bar, 1 mm. (b) Left-side view of tail region, including the notochord (no) and dorsal nerve cord (dnc) with its organs of Hesse (tandem arrow) and a dorsally-bent posterior extremity (single arrow). The asterisk marks the forward-facing point of a chevron. Scale line, 100 μm.

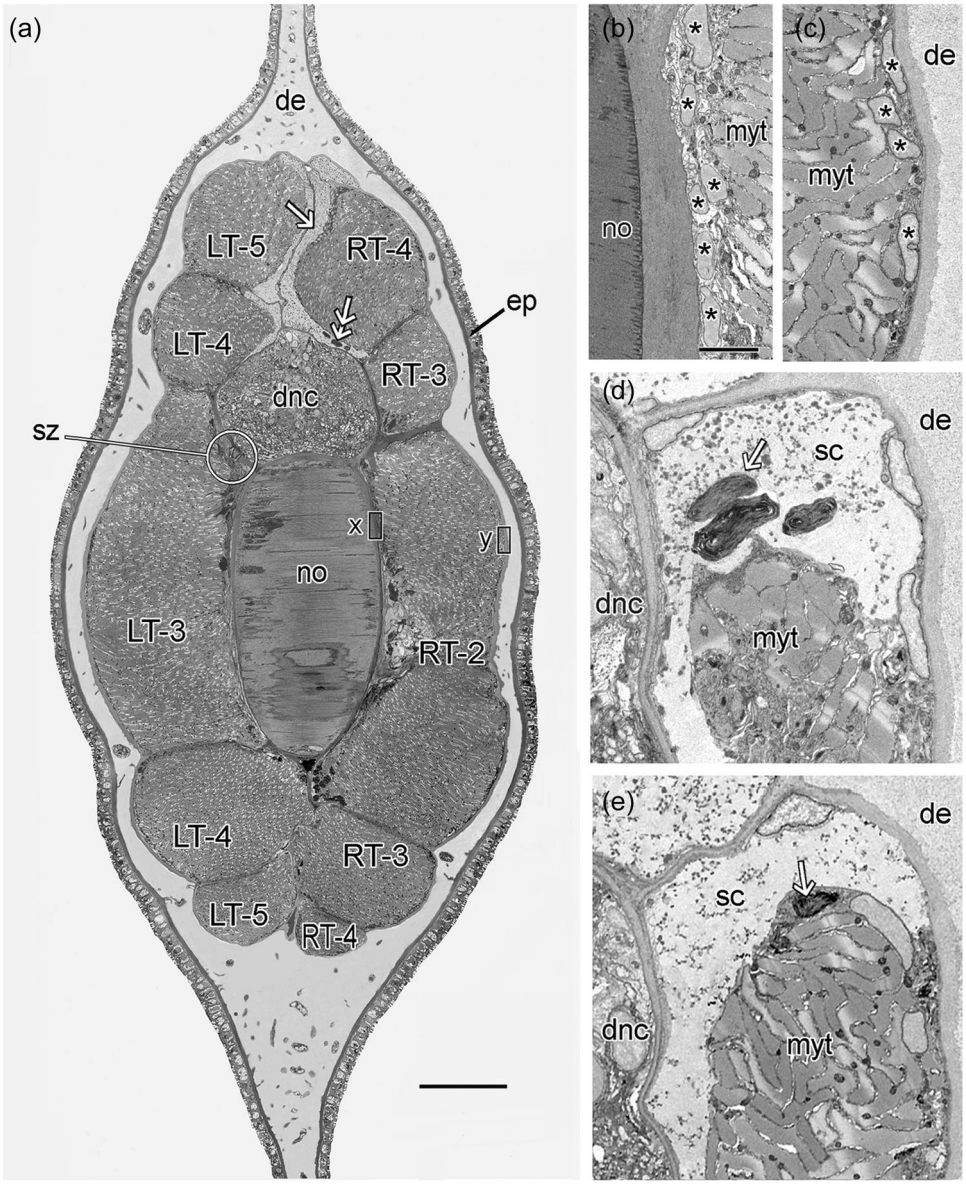

FIGURE 3 *Branchiostoma floridae*. (a) Montage of SBSEM images of the most anterior block-face (number 3200). The numbering system for the myomeres is explained in Section 2.2. Here, the same designation dorsally and ventrally identifies the two posterior-pointing limbs of a given chevron-shaped myomere. Other abbreviations from top are: de, dermis; ep, epidermis; dnc, dorsal nerve cord; sz, synaptic zone between muscle tails and nervous system; no, notochord. Single arrow indicates region of dilated sclerocoel; tandem arrows indicate large inclusions in sclerocoel. Scale bar, 50 μm. (b) Enlargement of rectangle x in 3a, showing notochord (no), sclerotome nuclei (asterisks), and myotome (myt). Scale bar (also applicable to c–e), 5 μm. (c) Enlargement of rectangle y in 3a, showing myotome (myt), dermatome nuclei (asterisks), and dermis (de). (d) Dilation of sclerocoel (sc) containing numerous small dense spheres and a few large inclusions (arrow). Other abbreviations are dorsal nerve cord (dnc), myotome (myt), and dermis (de). (e) Similar to 3d, but showing a sclerotome cell with dense material intracellularly (arrow), probably destined to be secreted as one of the large inclusions. SBSEM, serial block-face scanning electron microscopy.

In the enlargement, the most conspicuous tissues are the notochord and dorsal nerve cord. The latter, which includes some pigmented organs of Hesse (tandem arrows), is deflected dorsally at its posterior end (a normal feature of the anatomy according to Retzius, 1895). The boundaries of the chevron-shaped myomeres are visible anteriorly (toward left). An odd feature of amphioxus is that the left series of myomeres is offset half a segment anterior to the right series (Kuznetsov, 2023), and this, combined with both series showing simultaneously in the nearly transparent animal, makes the myomeres seem twice as narrow and twice as numerous as they should be. In any event, the myomere boundaries become less and less distinct as one proceeds posteriorly until they can no longer be visualized near the tail tip, although, as shown by SBSEM, several additional myomeres are present there (described in Sections 3.3 and 3.4). As an aside, in spite of the anterior half-segment offset on the left side, mentioned above, the right and left segment series of

amphioxus terminate at the tail end in register due to the cumulative effect of the irregular lengths of the myomeres at the posterior end.

3.2 | Montaged overview with special attention to the distended sclerocoel

Figure 3a is an overview of the most anterior block face we exposed (about halfway along the series of postanal myomeres). Conspicuous features are notochord, dorsal nerve cord, myotomal parts of the myomeres, dermis, epidermis, and some distended regions of sclerocoel (indicated by single arrows). In addition to these obvious structures, there are others that are difficult or impossible to visualize with SBSEM with its relatively low resolution. These poorly resolved structures were the extremely squamous cytoplasmic portions of the mesothelia comprising the dermatome and many regions of sclerotome (and the myocoels and the sclerocoels they respectively border). In many places, only the nuclear regions of such mesothelia are visible (Figure 3b,c, asterisks). Fortunately for interpretation of the present results, numerous studies with conventional TEM (Holland & Holland, 1990; Mansfield et al., 2015; Ruppert, 1997), have shown that sclerocoels and myocoels are located, respectively, medially and laterally in the myomeres.

Although, as mentioned above, the sclerocoel in some places is difficult to demonstrate, there are other regions where this structure is conspicuous because it is strikingly distended (Figure 3a). The coelomic fluid in these prominent spaces contains numerous, dense spheres, about 100–500 nm in diameter (Figure 3d) as well as considerably fewer, but much larger inclusions (about 5–10 µm in their long axis) consisting of compacted whorls of material of several densities (Figure 3d, single arrow). Such inclusions are evidently produced by mesothelial cells (Figure 3e, arrow) bordering the sclerocoel and then released into the lumen. There is a good possibility that the large inclusions break down into the multiplicity of small spheres. In any case, the presence of both kinds of formed elements is useful for distinguishing the sclerocoel from other spaces. In passing, we should mention that we detected no coelomocytes in the distended regions of sclerocoel, a finding consistent with the suspicion of Ruppert (1997) that Rhodes et al. (1982) were mistaken in claiming that such cells occur in amphioxus.

One additional feature notable in Figure 3a is a synaptic zone (sz) where cytoplasmic tails extending from the muscle cells in myotome LT−3 form synapses with neurons at the periphery of the dorsal nerve cord (as first demonstrated by Flood, 1966). This arrangement contrasts with the situation in vertebrates where axons of motor neurons exit the dorsal nerve cord as ventral roots and run a considerable distance before synapsing on muscle fibers.

3.3 | Left posterior myomeres: SBSEM reconstructions in 3D and histology

Figure 4a shows the most posterior myomeres on the left side with their usual 3D relations intact, whereas Figure 4b shows them separated to facilitate indicating the locations of block-face images in Figure 5. The conventions for naming these myomeres are explained above, in Section 2.2 of the materials and methods.

The LT myomere (LT) is a hollow vesicle enclosed everywhere by an envelope of undifferentiated looking cells (Figure 5a). In contrast, myomere LT-1 (Figure 4a,b), although less than half as

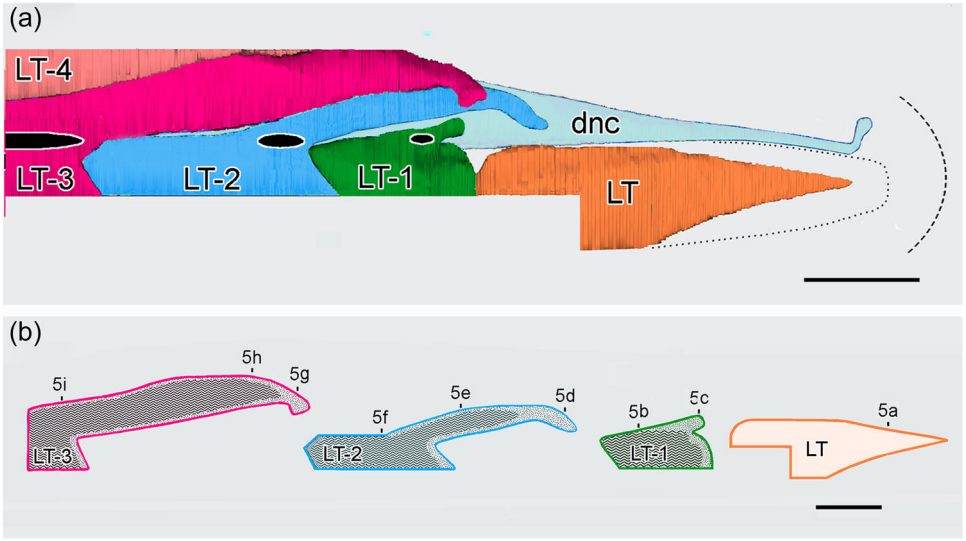

FIGURE 4 *Branchiostoma floridae*. (a) The five most posterior myomeres on the left side, from LT (left terminal) through LT−4 (left terminal minus four). Black ovals are synaptic zones between muscle tails on medial side of myomere and the dorsal neve cord (dnc). Posterior positions of notochord and epidermis are indicated, respectively, by dotted curves and dashed curves. Scale bar, 100 µm. (b) Same left-side myomeres but separated and showing regions of myotome (herringbone pattern) and sclerotome (stippling). Scale bar, 100 µm. Positions of block-face images in Figure 5 are indicated.

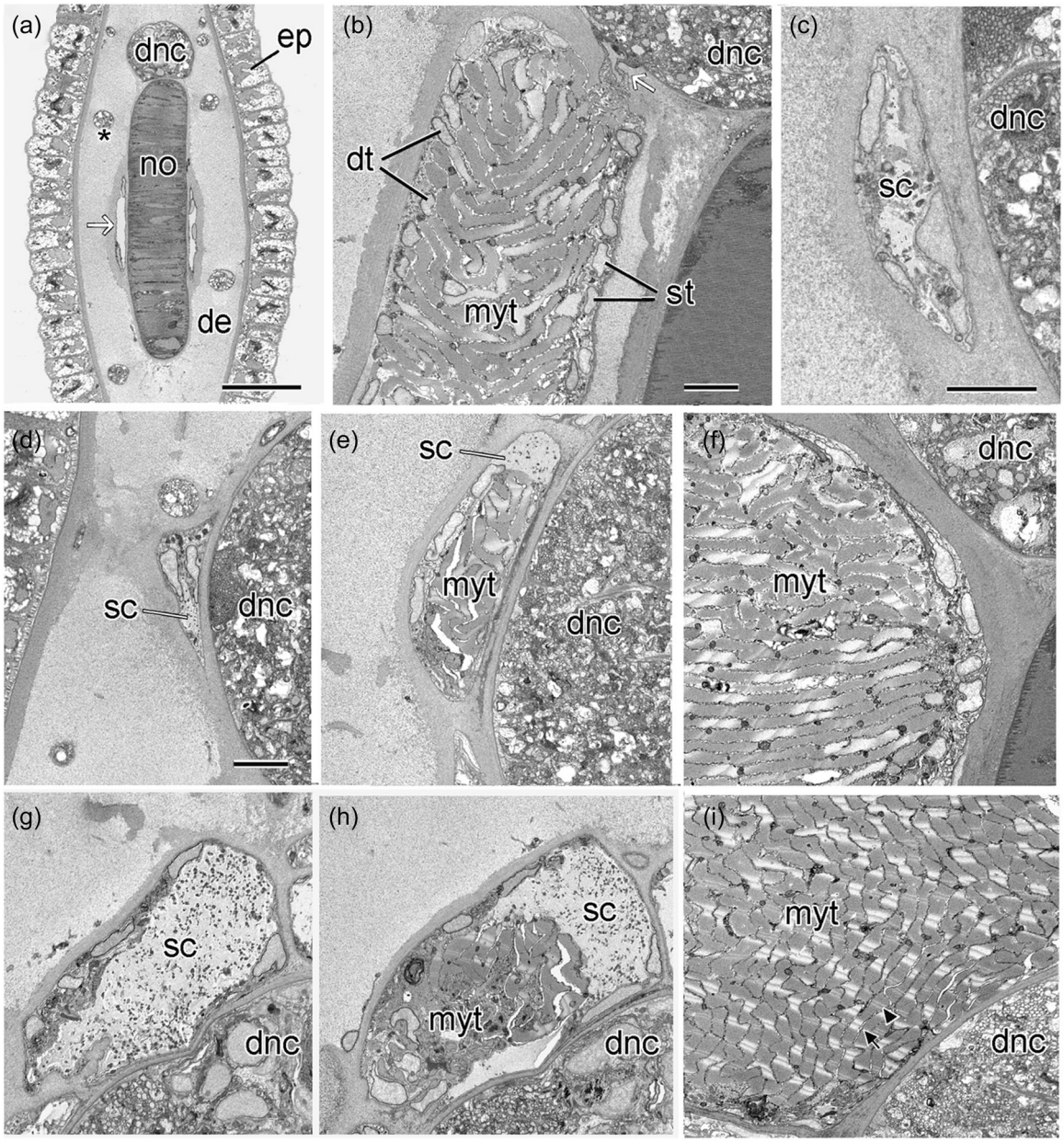

FIGURE 5 *Branchiostoma floridae*. Block-face images at transverse levels indicated in Figure 4b. (a) Posterior region of body showing myocoel (arrow) of myomere LT. Dermis, de; dorsal nerve cord, dnc; epidermis, ep; notochord, no; the asterisk marks a transverse view of a peripheral sensory nerve. Scale bar, 20 µm. (b) Main (ventral) part of LT-1 comprising the full spectrum of myomere structures—from medial to lateral, these are two mesothelia of sclerotome (st) enclosing a sclerocoel, a conspicuous myotome (myt), myocoel, and dermatome (dt). Scale bar 5 µm. (c) Transverse view of the sclerocoel (sc) in the nipple-like outgrowth of myomere LT−1 closely associated with the dorsal nerve cord (dnc). Scale bar, 5 µm. (d) Tip of dorsal limb of LT−2 adjacent to dorsal nerve cord (dnc) and comprising sclerotome surrounding small sclerocoel (sc). Scale bar, (also applicable to e through i), 5 µm. (e) Dorsal limb of chevron of LT−2 adjacent dorsal nerve cord (dnc); halfway along limb, the myotome (myt) predominates over the sclerotome (sclerocoel labeled sc). (f) Conspicuous myotome (myt) in ventral limb of LT−2 adjacent to dorsal nerve cord (dnc). (g) Tip of dorsal limb of chevron of LT−3, consisting entirely of sclerotome mesothelium enclosing scerocoel (sc). (h) Dorsal limb of chevron of LT−3 comprising both sclerotome (sc) and myotome (myt). (i) Ventral portion of LT−3 with prominent myotome composed of muscle cells with well-developed Z-lines (arrow) and H-zones (arrowhead).

long as LT (Figure 4a,b), includes differentiated tissues along its entire length. As discussed in Section 2.3, the location of the main, sac-like portion of LT-1 is ventral. However, from the dorsal side of this sac, a short, nipple-like structure arises and projects dorso-posteriorly. It is likely that this nipple represents the beginnings of formation of a dorsal limb of a chevron from the ventral limb (although, as mentioned in the introduction, it is important to remember that the morphology of LT−1 is evidently static and not a precursor of later developmental stages in post-metamorphic amphioxus). The main ventral part of LT−1

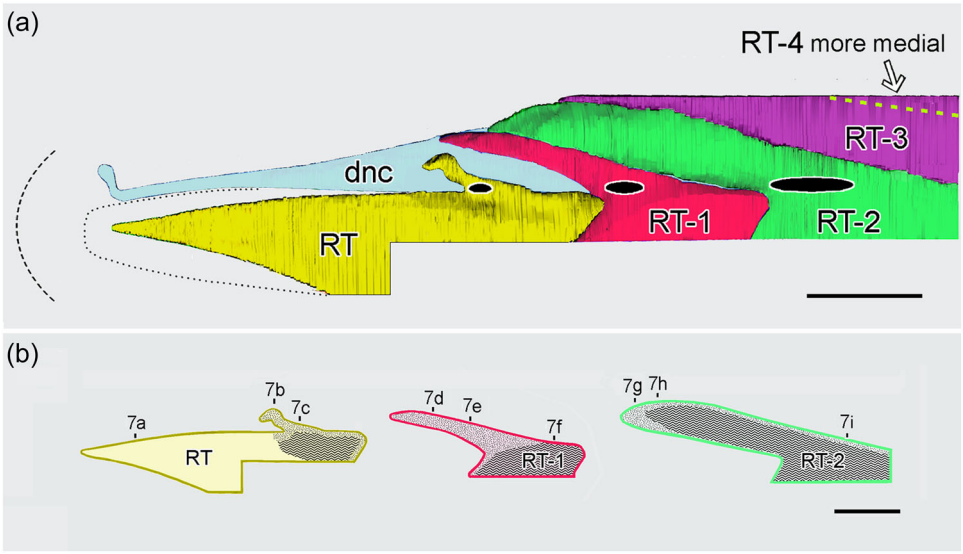

FIGURE 6 *Branchiostoma floridae*. (a) The five most posterior myomeres from RT (right terminal) through RT−4 (right terminal minus four); symbols as in 4a. Scale bar, 100 µm. (b) Same right-side myomeres but separated and showing regions of myotome (herringbone pattern) and sclerotome (stippling). Positions of block-face images in Figure 7 are indicated. Scale bar, 100 µm.

(Figure 5c) comprises the full spectrum of myomere structures—although, for reasons mentioned in Section 3.2, only the myotome is conspicuous. The constituent muscle cells, although the same size as differentiated amphioxus muscles, lacked Z-lines and H-zones. Presumably, therefore, they are not functional, although at least some of them extend muscle tails (Figure 5b, arrow) to a sz at the periphery of the dorsal nerve cord (dnc). Such sz are present on the remaining left-side myomeres and on all the right-side myomeres (to be covered in Section 3.4). In contrast to the ventral region of LT−1, the nipple arising from its dorsal side is composed entirely of sclerotome (Figure 5c).

In the LT−2 myomere, the dorsal limb of the chevron (Figure 4a,b) is much longer than in LT−1, although in transverse view (Figure 5d,e), it appears as a relatively insubstantial medio-laterally compressed strap. The tip of the projection consists entirely of sclerotome, while the more proximal regions contained both sclerotome and myotome. In the more substantial ventral limb of the chevron (Figure 5f), the myotome is the dominant component in the myomere and comprises muscle cells lacking H-zones, although indistinct Z-lines are detectable.

In the LT−3 myomere (Figure 4a,b), the dorsal limb of the chevron is relatively robust. Close to its distal tip, the only tissue present is distended sclerotome surrounding a spacious sclerocoel (Figure 5g). However, more proximally, a myotome appears (Figure 5h) and soon predominates in the dorsal limb. In the ventral limb, the most conspicuous feature is the myotome (Figure 5i), which is composed of presumably functional muscle cells characterized by well-developed Z-lines (arrow) and H-Zones (arrowhead).

3.4 | Right posterior myomeres: SBSEM reconstructions in 3D and histology

Figure 6a shows the most posterior myomeres on the right side with their usual 3D relations intact, whereas Figure 6b shows them separated to facilitate indicating the locations of block-face images in Figure 7. The naming of these myomeres, from posterior to anterior, has already been explained in Section 2.2

Like its counterpart on the left side of the animal, the right terminal myomere (RT) is enclosed posteriorly by a mesothelium of undifferentiated-looking cells (Figures 6b and 7a).

However, toward its anterior end, RT has a complex over-all shape and histology. The myomere gives rise to a nipple-like projection dorso-posteriorly (Figure 6a,b) that consists entirely of sclerotome (Figure 7b). In contrast to the nipple-like region, the main ventral module of RT (Figures 6b and 7c) includes all the tissues characteristic of a myomere, most conspicuously a myotome composed of muscle cells that presumably are not functional since they lack Z-lines or H-zones.

In comparison with the RT myomere, RT-1 bears a much longer dorsal outgrowth, possibly comparable to a thin dorsal limb of a chevron (Figure 6a,b). The entire outgrowth is composed of sclerotome (Figure 7d,e). The more substantial ventral region of the myomere (Figure 7f), although partially cut away, appears to be relatively sac-like with little if any part equivalent to the ventral limb of a chevron. In this region, myotome predominates and comprises muscle cells with both Z-lines and H-zones.

As one proceeds even farther anteriorly, the RT-2 myomere includes a relatively robust equivalent of the dorsal limb of a chevron

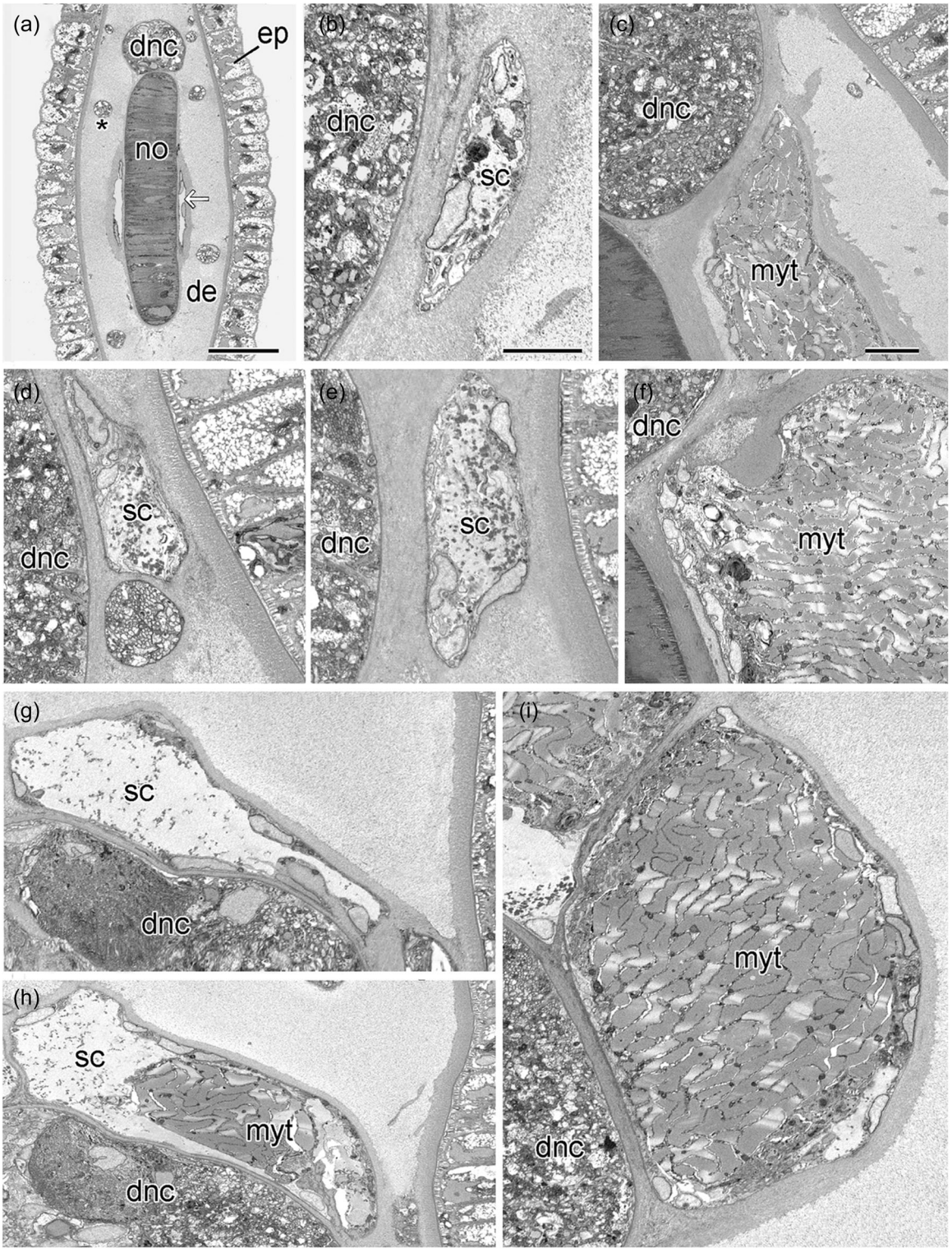

FIGURE 7 *Branchiostoma floridae*. Block-face images at transverse levels indicated in Figure 6b. In all images dnc indicates dorsal nerve cord. (a) Posterior region of myomere RT showing myocoel (arrow). Dermis, de; epidermis, ep; notochord, no; asterisk marks a transverse profile of a peripheral sensory nerve. Scale bar, 20 µm. (b) The anterior region of RT bears a small, nipple-like protrusion consisting entirely of sclerotome-enclosed sclerocoel (sc). Scale bar, 5 µm. (c) The anterior region of RT, which might correspond to the ventral limb of a chevron, includes a myotome (myt) and less conspicuous tissues of sclerotome and dermatome. Scale bar (also applicable to d through i), 5 µm. (d, e) RT−1 includes a possible equivalent of the dorsal limb of a chevron in the form of a long, strap-like protrusion of sclerotome-enclosed sclerocoel (sc). (f) The ventral limb of RT−1 is composed of conspicuous myotome (myt) as well as the less obvious tissues of the myomere. (g, h) Myomere RT−2 has a relatively robust dorsal limb with a tip consisting entirely of distended sclerocoel (sc), although the rest of its length comprises a mixture of distended sclerocoel (sc) and myotome (myt). (i) In the region of RT−2 representing the ventral limb of the chevron, the predominant component is myotome (myt), although the less obvious tissues of the myomere are also present.

(Figure 6a,b). The far distal region of this projection consists entirely of dilated sclerotome (Figure 7g), but, more proximally, both myotome and dilated sclerotome are present (Figure 7h). In the ventral region of the myomere (Figure 7i), the myotome predominates, and its constituent muscle cells are characterized by prominent Z-lines and H-zones.

4 | DISCUSSION

4.1 | Somite origin and myomere differentiation: Amphioxus versus vertebrates

Amphioxus and vertebrate somites originate somewhat differently. Those of amphioxus arise directly from precursor tissues (Beaster-Jones et al., 2008), whereas those of vertebrates are formed with less immediacy from the anterior end of a band of presomitic mesoderm cells generated by progenitors in the posterior tail bud (Fior et al., 2012). Another unusual feature of amphioxus somitogenesis is that, as the embryonic and larval body lengthens posteriorly, the somites apparently originate from a succession of tissue types. Here, for convenience, we have distinguished these origins as phases I-IV.

During phase I (Figure 1a), starting far anteriorly in the animal, somites with enterocoelic myocoels begin evaginating from the gut. Then, during phase II, the somites delaminate as a solid cluster of cells from the wall of the neurenteric canal (a connection between the neurocoele and hindgut); shortly thereafter, they open up myocoels by schizocoely. These two early stages have been extensively studied (Aldea et al., 2019; Beaster-Jones et al., 2008; Gostling & Shimeld, 2003; Hatschek, 1882; Mansfield et al., 2015; Onai et al., 2015; Schubert et al., 2001; Yong et al., 2021).

Near the transition from phase II to phase III, each somite increases in histological complexity to become a myomere consisting of two associated cellular envelopes (Figure 1b). The first envelope comprises mesothelia of the myotome and dermatome, which together enclose the myocoels; and the second comprises the medial and lateral mesothelia of the sclerotome, which together enclose the sclerocoel. Also, about this time, the myomeres morph into a chevron shape with a forward-facing point (already mentioned in Section 2.3). To date, amphioxus biologists have almost completely ignored how the chevrons form. In addition, nothing definite is known about somitogenesis during phase III (after the neurenteric canal has disappeared) or phase IV (in the absence of any endodermal tissue in the postanal region of the body).

4.2 | Transition from compact somite to chevron-shaped myomere

The earliest illustration of adult amphioxus was drawn by Pallas (1774), who included the conspicuous chevron-shaped myomeres, although he did not speculate on their identity. Subsequently, Hatschek (1882) showed that somites originated in amphioxus embryos as small spherical (or slightly oblong) groups of cells. Taken together, these two papers suffice to raise the question of how relatively uncomplicated somites can develop into chevron-shaped myomeres. Surprisingly, during the next 140 years, this has never been seriously addressed. All that is known is incidental information from the scanning electron microscopy of Stokes (1996) and conventional TEM of Mansfield et al. (2015). Both studies illustrate a rather abrupt dorso-ventral extension of the myomere plus its assumption of a chevron shape around the fourth day of development of *B. floridae*. Moreover, the only speculation on a mechanism for generating such chevrons was by Lacalli (2012), who suggested that muscle cell elongation within the myotome might provide part of the needed force.

At least superficially, the morphing of a relatively simple somite into a chevron shape seems similar in amphioxus and developing fishes. For zebrafish, this process has been examined over the past few decades with ever-increasing levels of sophistication, most recently by Tlili et al. (2019), a study combining live imaging of injected probes to quantify cell-level shape changes and movements in wild type and in genetically perturbed embryos. In addition, these data were used to inform theoretical modeling of mechanical processes on several spatial scales within the developing myomeres and between them and neighboring tissues. Although it would be desirable extend such methods for elucidating chevron formation in amphioxus, the excruciatingly small size of amphioxus larvae creates a problem for injection of molecular probes. The magnitude of this difficulty can be dramatized by comparing the sizes of developing amphioxus and zebrafish (minus its yolk mass) at the initiation of chevron formation—6 days at 30°C for amphioxus (Stokes, 1996) and 18 h at 28.5°C for the fish (Kimmel et al., 1995). At this stage, the volume of the fish is approximately 2000 times that of the amphioxus!

An additional aspect of chevron formation in amphioxus is whether the odd shaped, posterior myomeres indicate an alternative to the scenario of dorso-ventral extension-cum-assumption of a chevron shape. By looking at the posterior myomeres in Figures 5 and 7 in the order RT, LT−1, RT−1, LT−2, RT−2, one could imagine that the least modified myomere representing the ventral limb of a chevron produces a small bud that progressively enlarges to become the dorsal limb. Such a sequence would likely involve quite different underlying genetics and cell biology from those involved in the dorso-ventral extension and assumption of a chevron shape by the myomeres all along the more anterior regions of the amphioxus body. Even from the little that is known about chevron formation along most of the long axis of the amphioxus body, it appears that no such budding of a dorsal limb from a ventral limb of a chevron occurs there; if it did, the phenomenon probably would have been reported years ago. Therefore, until more is learned about the subject, it seems most prudent to consider chevron formation by dorsal budding to be a derived peculiarity limited to the posteriormost myomeres.

4.3 | Sclerotome and sclerocoel formation

Previous studies of cephalochordate sclerotome formation have been focused on myomeres along the greater part of the long axis of the body. Each such myomere includes a sclerocoel intervening between the myotome and the body axis (nerve cord and notochord). Such sclerocoels range from narrow to moderately inflated. During development, these sclerocoels do not originate until after the myotome is well differentiated. Hatschek (1882) proposed that the sclerotome arose by an evagination of the myotome wall, and this notion still survives in many textbooks. However, Mansfield et al. (2015) showed that, along most of the body length, presumably undifferentiated cells in the myotome wall form a monolayered sheet that intrudes between the myotome and axial structures (notochord and central nervous system) and then splits into the axial and lateral sclerotome mesothelia enclosing a sclerocoel.

In contrast to the typical sclerotome formation considered above, the present study suggests that the odd-shaped posterior myomeres produce their sclerotome somewhat differently. Thus, if one repeats the exercise of Section 4.1 by looking sequentially at LT and then at RT & LT−1, and then at RT−1 one sees that the dorsal limb of the chevron is at first an extensive outgrowth of pure sclerotome from the ventral limb. It is only at the next step (RT−2 & LT−2) that the myotome appears in the dorsal limb (perhaps differentiating in situ there from undifferentiated mesoderm cells). Because encroachment of the myotome stops short of the distal end of the dorsal limb, a distal region of sclerotome remains, surrounding a conspicuously dilated sclerocoel filled with an extracellular matrix including abundant small dense spheres and a few larger inclusions.

4.4 | Sclerocoel functions

Yong and Yu (2017) have discussed how a chordate ancestor of the vertebrates might have started with a sclerocoel containing an organic extracellular matrix and then co-opted mineralizing genes to mineralize the region, thereby innovating the skeletal system of vertebrates. However, in the present discussion, we will limit ourselves to the narrower question of how the contemporary, non-mineralized sclerocoel might function in extant cephalochordates. It has been suggested that amphioxus sclerocoels include lubricants that partly decouple the myotomes from the nerve cord and notochord during undulatory swimming (Franz, 1925; Holland & Holland, 1990; Ruppert, 1997; Sunnier, 1911), although no quantitative, biomechanical studies yet support this idea. In the present study, we found that the most extensive regions of distended sclerocoel in the amphioxus body were associated with the more posterior myomeres of the postanal series. The cross-sectional montage halfway through this region (Figure 2a) shows that enlarged sclerocoels are especially prominent dorsal to the central nervous system. Moreover, conspicuous sclerocoels were also associated with the dorsal limb of several of the odd-shaped myomeres at the extreme tail end of the animal. Collectively, the voluminous sclerocoels might help protect the posterior end of the central nervous system from physical trauma—for instance, when the amphioxus vigorously burrows into the substratum tail first.

4.5 | Odd-shaped posterior myomeres: How common in cephalochordates?

There are three genera of cephalochordates: *Asymmetron* and its sister group comprising *Epigonichthys* and *Branchiostoma* (Kon et al., 2007; Nishikawa, 2004, and see acknowledgments). Within each genus, one of the characters helping to identify post metamorphic specimens to species is the total number of myomeres per side (Poss & Boschung, 1996). Lankester (1889) was the first to worry about the accuracy of such counts. In his study of *Branchiostoma lanceolatum*, he reported that the last myomere was "by no means easy to count." To make matters worse, his illustrations show that what he thought was the last myomere was chevron-shaped. He, therefore, had no inkling that there were two or three additional myomeres even farther posterior. As mentioned in Section 2.2 it is quite possible that all species of *Branchiostoma* have similar posterior myomeres. Therefore, Lankester's inaccurate counting has almost certainly been repeated by every taxonomist using light microscopy to classify other *Branchiostoma* species (because all the counts have been incorrect to the same degree and in the same direction, no serious harm has resulted).

For the remaining cephalochordates, genus *Epigonichthys* is too poorly studied in all aspects of its biology to permit speculation on the presence of oddly-shaped posterior myomeres. However, more can be said about the genus *Asymmetron*, in which the adult tail continues as a thin caudal process (15% of the entire body length). The caudal process includes mesodermal cells clinging in small clusters to the right, ventral, and left sides of the notochordal sheath (Holland et al., 2022). It is likely that these cells represent part of a posteriormost somite (or paired somites) that might be a continuation of the postanal somite series, although this possibility remains to be examined.

5 | CONCLUSIONS

SBSEM can not only reveal new details about already-known cell types (Holland, 2021) but, as in the present study, can discover entirely new cell types that were overlooked in earlier studies with less incisive methods. Although the posteriormost myomeres discovered here in post-metamorphic specimens of amphioxus are structurally interesting, their functional significance, if any, is not clear. It is very unlikely that they make any contribution to undulatory swimming, because they are located at the extreme posterior end of the body, and many of them have a myotome comprising poorly differentiated muscle cells. Their conspicuously voluminous sclerocoels suggest they afford physical protection to the posterior end of

the central nervous system, but there is no experimental support for this idea. A particularly interesting feature of the posteriormost myomeres is their possible assumption of a chevron shape by budding off the dorsal limb of the chevron from the ventral limb. This contrasts with all the more anterior myomeres in the body (which, at least superficially, form chevrons after the fashion of fishes). Surprisingly, chevron formation in amphioxus has been almost entirely ignored by amphioxus biologists, and it would be interesting to look harder at the subject with modern methods.

AUTHOR CONTRIBUTIONS

Nicholas D. Holland: Conceptualization; funding acquisition, data collection and curation; 3D reconstructions; writing and editing. **Linda Z. Holland:** Conceptualization; funding acquisition; maintenance of breeding colony of *Branchiostoma floridae* at Scripps Institution of Oceanography; writing and editing.

ACKNOWLEDGMENTS

Jennifer Santini and Marcella Erb of the UCSD School of Medicine Microscopy Core assisted with both specimen fixation and operation of the SBSEM. The SBSEM facility and staff support are funded by the UCSD School of Medicine Microscopy Core Grants P30-NS047101 and OD030505. At Scripps Institution of Oceanography, support for amphioxus research comes from NSF Grant IOS 1952567 to Linda Z. Holland and Nicholas D. Holland. We would like to take this opportunity to apologize to Teruaki Nishikawa for our mistake in 2010 in the *Biological Bulletin*, *219*,122-141, wherein we carelessly misinterpreted his correct arrangement of the *Cephalochordate* genera.

CONFLICT OF INTEREST STATEMENT

The authors declare no conflict of interest.

DATA AVAILABILITY STATEMENT

The data that support the findings of this study are available on request from the corresponding author. The data are not publicly available due to privacy or ethical restrictions.

ORCID

Nicholas D. Holland http://orcid.org/0000-0002-3448-490X
Linda Z. Holland http://orcid.org/0000-0003-2960-9437

REFERENCES

Aldea, D., Subirana, L., Keime, C., Meister, L., Maeso, I., Marcellini, S., Gomez-Skarmeta, J. L., Bertrand, S., & Escriva, H. (2019). Genetic regulation of amphioxus somitogenesis informs the evolution of the vertebrate head mesoderm. *Nature Ecology & Evolution*, *3*, 1233–1240.

Beaster-Jones, L., Kaltenbach, S. L., Koop, D., Yuan, S., Chastain, R., & Holland, L. Z. (2008). Expression of somite segmentation genes in amphioxus: A clock without a wavefront? *Development Genes and Evolution*, *218*, 599–611.

Borrett, S., & Hughes, L. (2016). Reporting methods for processing and analysis of data from serial block face scanning electron microscopy. *Journal of Microscopy*, *263*, 3–9.

Carvalho, J. E., Lahye, F., Yong, L. W., Croce, J., Esciva, H., Yu, J. K., & Schubert, M. (2021). An updated staging system for cephalochordate development: One table suits them all. *BMC Biology*, *19*, 668006.

Deerinck, T. J., Bushong, E. A., Lev-Ram, Y., Shu, X., Tsien, R. Y., & Elisman, M. H. (2010). Enhancing serial block-face scanning electron microscopy to enable high resolution 3-D nanohistology of cells and tissues. *Microscopy & Microanalysis*, *16*, 1138–1139.

Delsuc, F., Tsagkogeorga, G., Lartillot, N., & Philippe, H. (2008). Additional molecular support for the new chordate phylogeny. *Genesis*, *46*, 592–604.

Fiala, J. C. (2005). Reconstruct: A free editor for serial section microscopy. *Journal of Microscopy*, *218*, 52–61.

Fior, R., Maxwell, A. A., Ma, T. P., Vezzaro, A., Moens, C. B., Amacher, S. L., Lewis, J., & Saúde, L. (2012). The differentiation and movement of presomitic mesoderm progenitor cells are controlled by *Mesogenin 1*. *Development*, *139*, 4656–4665.

Flood, P. R. (1966). A peculiar mode of muscular innervation in amphioxus. *The Journal of Comparative Neurology*, *126*, 181–217.

Franz, V. (1925). Morphologische und ontogenetische Akranierstudien über Darm, Trichter, Zölomderivate, Muskulatur- und Bindegewebsformationen. *Jenaische Zeitschrift für Naturwissenschaft*, *61*, 407–468.

Gostling, N. J., & Shimeld, S. M. (2003). Protochordate *Zic* genes define primitive somite compartments and highlight molecular changes underlying neural crest evolution. *Evolution & Development*, *5*, 136–144.

Hatschek, B. (1882). Studien über Entwickelung des Amphioxus. *Arbeiten aus dem zoologischen Instituten der Universität Wien und der zoologischen Station in Triest*, *4*, 1–88.

Holland, L. Z., & Li, G. (2021). Laboratory culture and mutagenesis of amphioxus. *Methods in Molecular Biology*, *2219*, 1–29.

Holland, N. D. (2021). Hunting needles in a haystack: Migrating precursors of epidermal sensory neurons in amphioxus found with serial blockface scanning electron microscopy (SBSEM). *Acta Zoologica*, *102*, 165–170.

Holland, N. D., & Holland, L. Z. (1990). Fine structure of the mesothelia and extracellular materials in the coelomic fluid of the fin boxes, myocoels and sclerocoels of a lancelet, *Branchiostoma floridae* (Cephalochordata = Acrania). *Acta Zoologica*, *71*, 225–234.

Holland, N. D., Holland, L. Z., & Somorjai, I. M. L. (2022). Three-dimensional fine structure of fibroblasts and other mesodermally derived tissues in the dermis of adults of the Bahamas lancelet (Chordata, Cephalohordata), as seen by serial block-face scanning electron microscopy. *Journal of Morphology*, *283*, 1289–1298.

Howell, W. M. (1964). Studies on the variation in a topotypic population of the lancelet, *Branchiostoma floridae*, from Tampa Bay, Florida. Master's thesis, University of Alabama.

Hubbs, C. L. (1922). A list of the lancelets of the world with diagnoses of five new species of Branchiostoma. *Occasional Papers of the Museum of Zoology*, *105*, 1–16.

Kimmel, C. B., Ballard, W. W., Kimmel, S. R., Ullmann, B., & Schilling, T. F. (1995). Stages of embryonic development of the zebrafish. *Developmental Dynamics*, *203*, 253–310.

Kon, T., Nohara, M., Yamanoue, Y., Fujiwara, Y., Nishida, M., & Nishikawa, T. (2007). Phylogenetic position of a whale-fall lancelet (Cephalochordata) inferred from whole mitochondrial genome sequences. *BMC Evolutionary Biology*, *7*, 127–132.

Kornfeld, J., & Denk, W. (2018). Progress and remaining challenges in high-throughput volume electron microscopy. *Current Opinion in Neurobiology*, *50*, 261–267.

Kuznetsov, A. N. (2023). Glide-reflection symmetry in deuterostomes: An evolutionary perspective. *Biological Journal of the Linnean Society*, *140*. Advance online publication.

Lacalli, T. (2012). More thoughts on notochords: An archived comment on: The Middle Cambrian fossil Pikaia and the evolution of chordate swimming. *EvoDevo*, *2*, 12.

Lankester, E. R. (1889). Contributions to the knowledge of *Amphioxus lanceolatus*, Yarrell. *Quarterly Journal of Microscopical Science*, *29*, 365–408.

Mansfield, J. H., Haller, E., Holland, N. D., & Brent, A. E. (2015). Development of somites and their derivatives in amphioxus, and implications for the evolution of vertebrate somites. *EvoDevo*, *6*, 21.

Nishikawa, T. (2004). A new deep-water lancelet (Cephalochordata) from off Cape Nomamisaki, SW Japan, with a proposal of the revised system recovering the genus *Asymmetron*. *Zoological Science*, *21*, 1131–1136.

Onai, T., Aramaki, T., Inomata, H., Hirai, T., & Kuratani, S. (2015). On the origin of vertebrate somites. *Zoological Letters*, *1*, 33.

Pallas, P. S. (1774). Spicilegia Zoologica, Volume *1*, Fascicle 10, Plate I, Figure 11. G. A. Lange.

Poss, S. G., & Boschung, H. T. (1996). Lancelets (Cephalochordata: Branchiostomatidae): How many species are valid? *Israel Journal of Zoology*, *42*, S13–S66.

Retzius, G. (1895). Das hintere Ende des Rückenmarkes und sein Verhalten zur Chorda dorsalis bei *Amphioxus lanceolatus*. *Biologische Untersuchungen*, *7*, 19–21.

Rhodes, C. P., Ratcliffe, N. A., & Rowley, A. F. (1982). Presence of coelomocytes in the primitive chordate amphioxus (*Branchiostoma lanceolatum*). *Science*, *217*, 263–265.

Ruppert, E. E. (1997). Cephalochordata (Acrania). In F. W. Harrison & E. E. Ruppert (Eds.), Microscopic Anatomy of invertebrates, *Volume 15*, *Hemichordata, Chaetognatha, and the invertebrate chordates* (pp. 349–505). Wiley-Liss.

Schubert, M., Holland, L. Z., Stokes, M. D., & Holland, N. D. (2001). Three amphioxus Wnt genes (AmphiWnt3, *AmphiWnt5*, and *AmphiWnt6*) associated with the tail bud: The evolution of somitogenesis in chordates. *Developmental Biology*, *240*, 262–273.

Somorjai, I., Bertrand, S., Camasses, A., Haguenauer, A., & Escriva, H. (2008). Evidence for stasis and not genetic piracy in developmental expression patterns of *Branchiostoma lanceolatum* and *Branchiostoma floridae*, two amphioxus species that have evolved independently over the course of 200 Myr. *Development Genes and Evolution*, *218*, 703–713.

Stokes, M. D. (1996). Ontogenetic changes in the morphology, ecology and locomotory biomechanics of the lancelet, *Branchiostoma floridae*. PhD Dissertation. Scripps Institution of Oceanography (University of California at San Diego).

Sunnier, A. L. J. (1911). Les premiers stades de la différentiation interne du myotome et la formation des éléments sclérotomatique chez les acraniens, les sélaciens et les téléostéens. *Onderzoekingen verricht in het zoologisch laboratorium der Rijksuniversiteit Groningen*, *2*, 1–109.

Tlili, S., Yin, J., Rupprecht, J. F., Mendieta-Serrano, M. A., Weissbart, G., Verma, N., Teng, X., Toyama, Y., Prost, J., & Saunders, T. E. (2019). Shaping the zebrafish myotome by intertissue friction and active stress. *Proceedings of the National Academy of Sciences*, *116*, 25430–25439.

Wanner, A. A., Genoud, C., & Friedrich, R. W. (2016). 3-dimensional electron microscopic imaging of the zebrafish olfactory bulb and dense reconstruction of neurons. *Scientific Data*, *3*, 160100.

Yong, L. W., Lu, T. M., Tung, C. H., Chiou, R. J., Li, K. L., & Yu, J. K. (2021). Somite compartments in amphioxus and its implications on the evolution of the vertebrate skeletal tissues. *Frontiers in Cell and Developmental Biology*, *9*, 607057.

Yong, L. W., & Yu, J. K. (2017). Tracing the evolutionary origin of vertebrate skeletal tissues: Insights from the cephalochordate amphioxus. *Current Opinion in Genetics & Development*, *39*, 55–62.

Yue, J. X., Yu, J. K., Putnam, N. H., & Holland, L. Z. (2014). The transcriptome of an amphioxus, *Asymmetron lucayanum*, from the Bahamas, a window into chordate evolution. *Genome Biology and Evolution*, *6*, 2681–2696.

How to cite this article: Holland, N. D., & Holland, L. Z. (2023). Serial block-face scanning electron microscopy of the tail tip of post-metamorphic amphioxus finds novel myomeres with odd shapes and unusually prominent sclerocoels. *Journal of Morphology*, *285*, e21667. https://doi.org/10.1002/jmor.21667